Research Article

Inducing Silver Nanoparticles on Supramolecular Functionalized Boron Nitride Nanosheets for Photocatalytic Removal of Reactive Blue Dyes

Adem Ali Muhabie [ID],[1] Beshir Legas Muhammed,[1] Mohammed Hussen Seid,[1] and Chih-Chia Cheng [ID][2]

[1]*Department of Chemistry, Faculty of Natural and Computational Sciences, Woldia University, Ethiopia*
[2]*Graduate Institute of Applied Science and Technology, National Taiwan University of Science and Technology, Taipei 10607, Taiwan*

Correspondence should be addressed to Adem Ali Muhabie; alimohabe2003@gmail.com
and Chih-Chia Cheng; cccheng@mail.ntust.edu.tw

A new hybrid nanomaterial has been developed by inducing catalytic silver nanoparticle on supramolecular BN nanosheets using supramolecular polymer as hybrid coordinator for photocatalytic removal of reactive blue dye (RB 221) from aqueous solution. In this study, adenine-bifunctionalized polypropylene glycol diacrylate (APPG) polymer was used for exfoliation and modification of BNNSs to decorate Ag nanoparticles that are prepared by sonication-assisted liquid phase exfoliation techniques. The synthesized materials are systematically characterized by various techniques such as FT-IR, UV-visible spectroscopy, Raman, FE-SEM, and HR-TEM. The layered structure of supramolecular polymer was observed over the exfoliated few layered BNNSs (2.0 to 3.5 nm). HR-TEM show that the silver nanoparticles (Ag NPs) were successfully decorated on supramolecular functionalized BN nanosheets. The significance of functionalization is that the adenine moieties induce the high amount of Ag NPs through Ag/adenine moiety coordination, thereby increasing the effectiveness of catalyst towards removal of RB 221 dye. The RB 221 dye removal efficiency of new synthesized nanomaterials such as BN/APPG/Ag (1 : 2.5), BN/APPG/Ag (1 : 1), APPG/Ag, and BN/Ag were $84.60 \pm 1.26\%$, 70.13 ± 0.034, 65.60 ± 0.052, and $35.0 \pm 0.45\%$, respectively. The photocatalytic dye degradation performance of catalyst increases with high amount of supramolecular polymer in the composites. Reusability of analysis revealed that regenerated BN/APPG/Ag catalyst could be tested in at least three consecutive cycles in which proving efficiency removal of the RB 221 was found to be 83.7 ± 0.8, 63.8 ± 0.51, and $54.60 \pm 0.78\%$ after the first, second, and third cycles of reuse, respectively. In addition, the absorption peaks of the RB 221 in solutions undergo upshifts relative to the free dye indicating the reduction of RB 221 dye for only BNNSs containing composite catalysts. Overall, the findings of this work are promising and therefore propose that BN/APPG/Ag could be applicable for the removal of dyes repeatedly for wastewater treatment in environment as result of their reusability and versatility.

1. Introduction

Hexagonal boron nitride nanosheets (h-BNNSs) are currently receiving enormous attention as nonoxide-layered nanomaterials, mainly because of their resistivity, sizable bandgap, and thermal, unique optical, mechanical, and chemical properties [1–3]. h-BNNSs can be used in many applications such as composites, drug delivery [4], filtration

technology, optical/electronic devices [5, 6], and catalyst support [7]. In addition, because of their high aspect ratio and nanoscale dimensions, h-BNNSs have a large surface morphology that may be used as supporter to achieve efficient catalytic processes and adsorption of environment pollutants. Few-layer BN nanosheet is more oxidation resistant and easily expected to be used as a support composite for small metal particles like Ag NPs on the surfaces; it has

large surface area, which adsorbed dense of particles to enhance photocatalytic degradation of dye. However, the complex fabrication process, low yield, restacking, reactivity, and solubility of h-BNNSs inhibit their use on a large scale [8]. These limitations cannot be occurred in the use of liquid phase exfoliation methods which is a promising approach to produce 2D nanomaterials in high structural quality and stable and uniform dispersions compared to the other synthesis methods of chemical vapor deposition, chemical, centrifugation, and mechanical exfoliation [9, 10]. In this respect, the simultaneous exfoliation and chemical functionalization with polymer have been achieved in the field of composite chemistry that enable the surface chemically reactive to bind nanoparticles for multifunctional purpose [4, 11]. The modification of the h-BNNSs surface by using covalent and noncovalent interactions will be allowed the rapid exfoliation of h-BN as a support for depositing metal nanoparticles (NP) as catalyst application for removal of dye environment [12, 13]. As dye removal represents a fundamental tool for improving the performance of several processes, the design of unique building blocks and NPs will attribute to the development of functionalized large surface area dye catalytic degradation [14]. In particular, decorated nanosheet capable with a high surface area allows high dye removal efficiency of activated surface. Recently, adenine-functionalized carbon nanotubes have been studied and anchor catalytic silver nanoparticles that were promising organic compound oxidation [15]. The strong nitrogen–NP bond allowed for simple anchoring of different chemical species to the surface of gold NPs, regardless of their molecular structure. Polystyrene has been used by researchers to deposit titania NPs for photodiscoloring methylene blue organic contaminants [16].

The growth of industrialization and the expansion of urbanization have a negative impact of discharge wastes into the environment [17]. The main toxin chemicals present in wastewater could be categorized as organic, inorganic, and biological that pollutes the environment. One of the common reasons of environmental contamination is the effluent from textile industry. The removal of dyes from industrial discharge is a key concern today and carries a great deal of importance. Anionic, cationic, and nonionic dyes are the three major classes of industrial dyes. Because of the several applications of anionic dye (basic and reactive dyes) in many industries, these have the chance to be discharged into the environment and can pollute bodies of water and have a deep influence by altering the biological cycles and affecting photosynthesis processes. Moreover, they can possibly threaten human health because prolonged contact with these products can lead to toxic reactions [18]. We have chosen the reactive blue dye 221 (RB 221) as a model dye to prove the removal efficiency of the new h-BNNSs/APPG/Ag two-dimensional (2D) nanomaterial as catalyst. Among reactive dyes, RB 221 is one of the organic pollutants regularly release from textile industries [17]. In addition to this, the dye has been used widely in different industries such as textile, leather treatment, paper/pulp manufacturing, plastics, and printing and could be a cause of serious ecological and water pollution problem in the world today [17, 19]. However, the decolorization of wastes of RB 221 dye is not exten-

sively studied by researchers, and it is very hard to remove the target dye from wastes [20].

Due to this reason, researches have been explored in order to remove organic pollutants to minimize the risks. Recently, the researchers have developed technology; adsorption, chemical oxidation, photocatalytic degradation, reduction, and membrane filtration have been applied to eliminate organic pollutants within wastewaters [21, 22]. However, the major difficulties of these technologies are management and disposal problems, high sludge production, technical limitations, and high cost and they are not environmentally friendly [23]. So far, the fabrication of cost-effective, efficient techniques is environmentally benign and is an important concern in the field of environmental chemistry [20]. Recently, NP-based catalysts have carried out the decolorization of organic pollutants. However, the use of precious metal nanoparticle material makes the catalyst expensive [17]. Moreover, the easy aggregation of metal nanoparticles limits their large-scale applications and therefore sometimes needs the catalyst support to prevent the dose usage and aggregation [23]. In order to avoid this problem, 2D semiconductor substrate could be triggered for treatment of organic pollutants in wastewater. Among these materials, BN nanosheet catalyst support attracts particular attention due to their high chemical inertness, high surface area, and low-cost and nontoxic nature. As far as authors know, no report has been yet reported about the supramolecular BN nanosheet coated with Ag NPs for catalytic reduction applications of organic pollutants because APPG is a new fabricated material.

Herein, we describe a simple, new methodology to design the growth of Ag NPs on the surface of h-BN by using the supramolecular polymer as particle coordinator and the use of the resulting nanomaterials as effective photocatalyst for the removal of reactive blue dye from aqueous solution. In the process of designing new BN/APPG/Ag, we focused our attention on using functional groups of adenine moiety that induce the growth of NPs directly at the surface of functionalized h-BNNSs. APPG is one of the supramolecular polymer that has been chosen for encapsulation of Ag NP particles because adenine moiety, a purine nucleobase, is endowed with suitable metal ion binding sites. Supramolecular polymer is thermoset, biodegradable, inert, and nontoxic [9, 24]. BN nanosheet is a supportive material for the catalyst of Ag nanoparticle. The new h-BN/APPG/Ag nanomaterials have been synthesized by the liquid phase exfoliation method, and Ag particles have been seeded on APPG using ultrasonication techniques. Therefore, the inspiration of the present work is to discover methods sensibly using the functionalized BN with APPG as a support for growth of Ag NPs for catalysts to adsorb or eliminate contaminants existing in the environment. The reusability of the developed photocatalysts was also investigated.

2. Experimental Procedures

2.1. Raw Materials. Poly(propylene glycol) diacrylate, adenine, silver nitrate, RB 221, layered hexagonal boron nitride, sodium boron hydride, and other chemicals were obtained

from Sigma-Aldrich (St. Louis, MO, USA) and applied without further purification. All solvents and reagents that were used in this research were analytical graded and purchased from TEDIA (Fairfield, OH, USA).

2.2. Preparation of BN Nanosheet with Supramolecular Polymer (APPG). Adenine-bifunctionalized poly(propylene glycol) diacrylate was synthesized from adenine and polypropylene glycol diacrylate (PPGDA) by using Michael addition reaction. The synthesis procedure is described in detail in our previous work [9]. The BN and the synthesized polymer APPG were mixed by different amount (BN/APPG, m/m, 0:1, 1:1, and 1:2.5 in ratio). The mixtures were added into vial containing 50 mL water and sonicated for eight hours at room temperature. After sonication, excess APPG polymers and unexfoliated BN were eliminated by centrifugation and then filtration. Finally, solution of dispersions was washed several times with water and dried and used for analysis.

2.3. Preparation of BN/APPG/Ag Nanocomposites. In a typical procedure, 200 mg of BN/APPG (0:1, 1:1, and 1:2.5 ratio in m/m) was first added to 30 mL of deionized water in a 100 mL vial and dispersed by ultrasonic treatment capped with magnetic stirrer at a 400 rpm for 3 min after completion of the dispersion. The deposition of Ag NPs on to the surface of samples was achieved by simple modification of the previous protocol as follows: the mixture solution $AgNO_3$ and methanol was added and stirred towards the reduction of Ag^+ upon the dropwise addition of $NaBH_4$ until the color changed to greenish yellow. The appearance of the greenish yellow color indicated the formation of BN/APPG/Ag nanocomposite, and the solution was continuously stirred for another 1 hr. The solution was then cooled to room temperature, and the final products were collected after centrifugation and washed with deionized water and pure ethanol at least three times. The resultant prepared nanomaterials were dried in a vacuum oven at a temperature of 55°C overnight to remove the absorbed water for the further characterizations. We prepared that it is possible to tailor the coordination of Ag NPs on to h-BNNSs surface by covalent functionalization of oxidized h-BNNSs with a modified adenine moiety.

2.4. Characterization Methods. Fourier transform infrared (FTIR) spectrometer measurement was conducted at a wave number range of 4000–600 cm^{-1} to explore the presence of functional groups within polymer grafted over nanomaterials. UV-vis spectrophotometer (Jasco V-550 type, Tokyo, Japan) experiment was performed to investigate the incorporation composites and the dye removal performance of catalysts. Raman spectra were recorded by using laser Raman spectrometer (Model CRM 2000; WITec Inc., Ulm, Germany) at 200 to 1600 cm^{-1} and room temperature. High-resolution transmission electron microscopy (TEM) (H-7000; Hitachi, Tokyo, Japan) and field emission scanning electron microscopy (FE-SEM) (JSM-6500F, JEOL, Japan) were conducted to investigate surface morphology and microstructure of prepared nanomaterials. To identify the

elements, present EDx measurement was performed. The resultant thicknesses and the lateral size (i.e., the length of sheet) and the appearance of exfoliated BN flakes were measured using an atomic force microscope (AFM) (NX10, Park Systems, Suwon, South Korea).

2.5. Photocatalytic Measurement. The experiments for investigating the photocatalytic activity of the as-prepared sheets were performed in a batch reactor that consisted of a glass Petri dish in which the 100 mg of as-synthesized catalyst was added. A RB 221 solution (100 mL) with a concentration of 5 mg L^{-1} was transferred into the dishes. Photocatalytic degradation of RB 221 in aqueous solution was carried out under UV light (254 nm) at the neutral pH of 7.4. Before irradiation, the solutions were placed in the dark for 2 hr to reach an adsorption-desorption equilibrium. Then, the solutions were irradiated in UV light of 100 W for 2 h. Eventually, the degradation progress of RB 221 by synthesized photocatalysts was examined at different intervals of time by a JASCO V-670 UV-visible spectrophotometer. For determination of the RB 221 concentration, a calibration graph ($R^2 = 0.9966$) was used. The percentage of dye removal efficiency of photocatalyst is calculated by [25]

$$x = \left(1 - \frac{C_t}{C_o}\right) \times 100\%, \tag{1}$$

where C_o is the initial concentration solution of RB 221 and C_t is the concentration of RB 221 during decolorization process within time interval.

3. Results and Discussion

To develop an easily manipulated hydrogen bond forming supramolecular polymer, we have been bifunctionalized poly(propylene glycol) diacrylate (APPDA) with adenine via Michael addition reaction using potassium tert-butoxide as a catalyst (Scheme 1(a)), reported in our previous work [9, 26]. Adenine is a nucleobase which can be a site for manipulating the polymers in different shapes and for multifunctional purposes [27], which enable to form spherical, layered sheet, and nanorode-like structure by either inter- or intradimerization of adenine moieties [24, 27–29]. In addition, adenine moieties would be binding site in order to trap a metal ion catalysts over nanosheet. Therefore, the pristine h-BN was simultaneously exfoliated and functionalized with adenine-PPG polymer by sonication techniques at room temperature in aqueous solution for eight hours (Scheme 1(b)). The exfoliated BN nanosheet was functionalized with the synthesized supramolecular polymer which might be due to the π-π interaction between hexagonal structure (aromatic resemble nature) of BN sheet and adenine ring in APPG polymer [4, 30]. Adenine moieties are not only increasing the stability and exfoliating extent but also it facilitates the solubility of the dispersions [31]. The BN flake dispersion in aqueous solution shows milky white solution; however, the color changed to the greenish yellow dispersion formed as result of bond coordination between adenine moieties and NPs

PPGDA

(a)

APPG

AgNO₃

Sonicate for 8 hr
Exfoliation & functionalization

H-BN

● = Ag   ⬡ = APPG

(b)
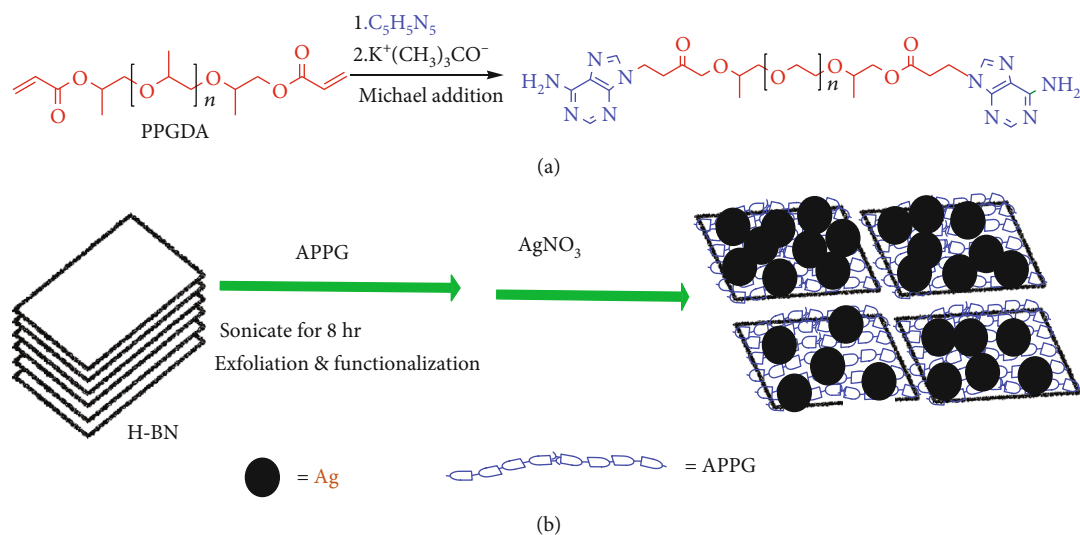
SCHEME 1: (a) The synthesis procedure of APPG supramolecular polymer. (b) Schematic illustration of the fabrication of BNNS-APPG-Ag hybrid nanomaterials in direct noncovalent liquid phase exfoliation technique.
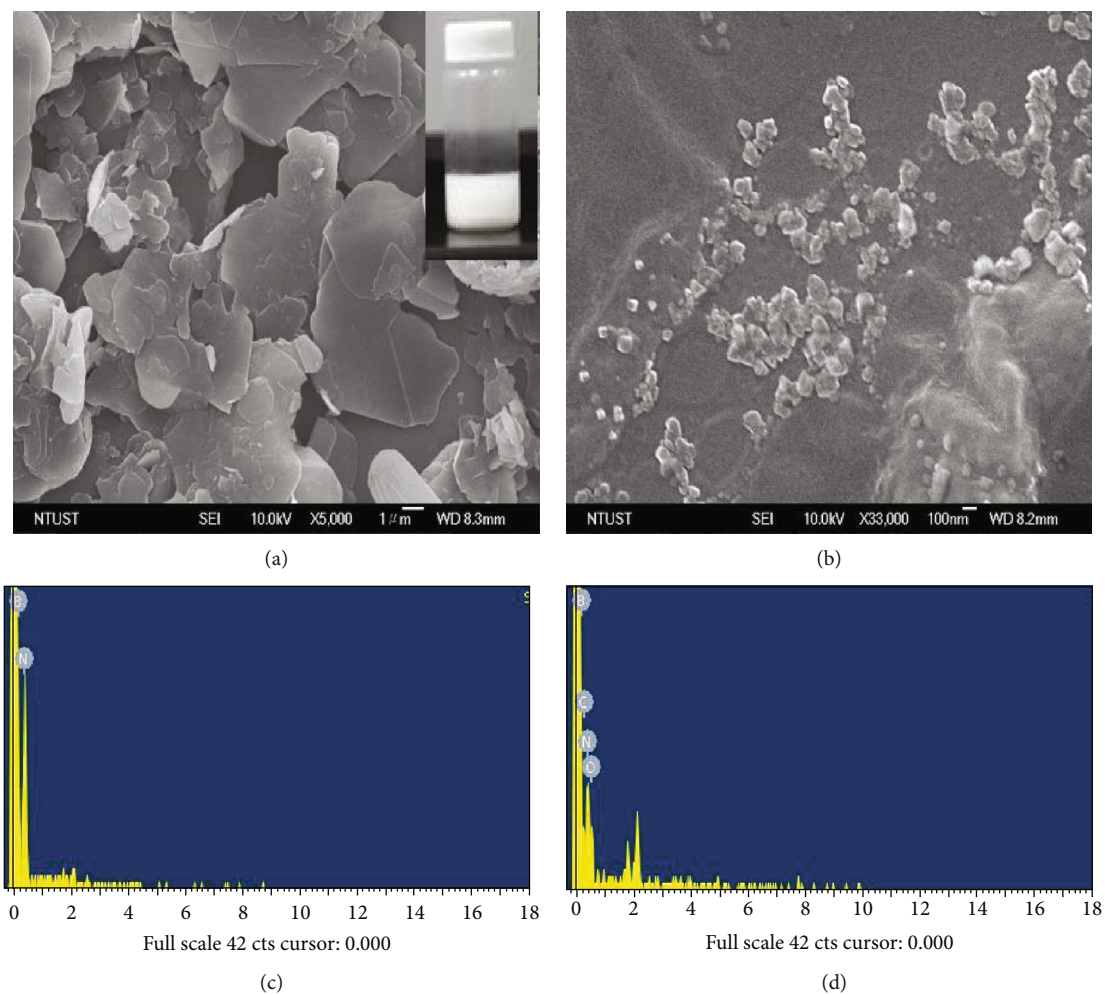

(a)

(b)

(c)

(d)

FIGURE 1: FE-SEM image of (a) h-BN and (b) h-BN/APPG/Ag corresponding to their EDS spectra of (c) and (b).
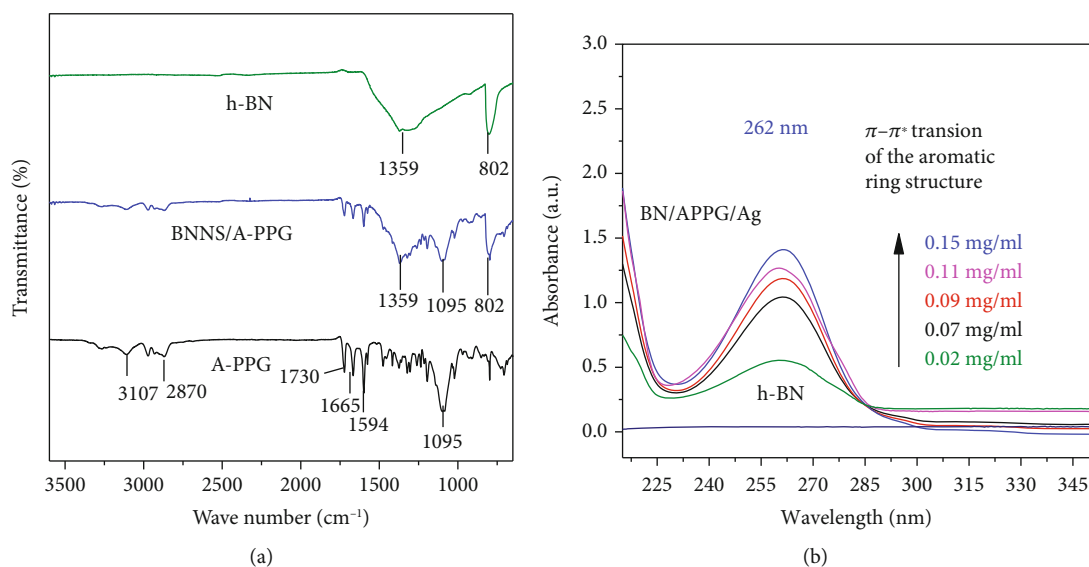
(a)

(b)

FIGURE 2: FT-IR absorption of APPG, h-BN, and BN/APPG (a). (b) UV-vis spectra of h-BN and h-BN/APPG with different concentrations.
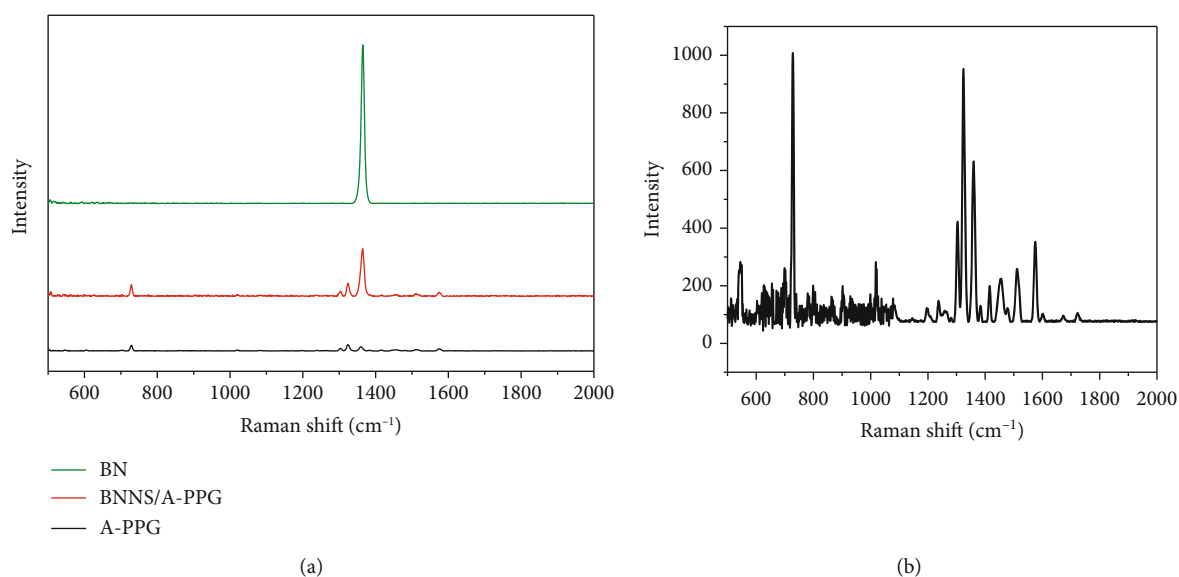

(a)

(b)

FIGURE 3: (a) Raman spectra for APPG, h-BN, and h-BN/APP. (b) Enlarged view of APPG Raman peaks.

(Figure 1). The BN/APPG nanosheets were dispersed in methanol solution of AgNO$_3$ and decorated with Ag nanoparticles. The deposition of NPs over the sheets occurred through the polymeric chain, nanoparticles coordinated to the amines and imine of adenine ring through by coordination chemistry [15].

The new BNNS-APPG-Ag hybrid nanomaterials were synthesized by simple, low-cost, and reliable sonication-assisted liquid phase exfoliation method. The dispersion in the solution was highly chemically stable, could not settled down more than month at room temperature, and illustrates no obvious sign of precipitation; the induction of NPs with polymer chain was used also to avoid noncovalent interactions between APPG polymers that may be the cause for restack of few layer nanosheets. The degree coverage of BN

flake with Ag NPs is based on the concentration of polymer grafted in which the adenine moiety binds metal nanoparticles [16]. The as-prepared catalysts were characterized by different techniques for photocatalytic removal of environment pollutant dye in this research. FTIR spectroscopy was one of the techniques employed to investigate the functionalization of BNNSs with polymer. FTIR spectra of h-BN, APPG, and BN/APPG composite are shown in Figure 2(a). The FTIR spectra of the APPG show a peaks at 3271 and 3110 cm^{-1} that can be assigned to the primary and secondary amine stretching vibration peaks [32]. The peaks at 1762, 1677, 1602, and 1092 cm^{-1} were ascribed to the absorption vibration peaks of C=O, C=N, C=C, and C-O bond, respectively. After exfoliation of h-BN by APPG macromere, a different typical vibration peaks were observed from h-BN.
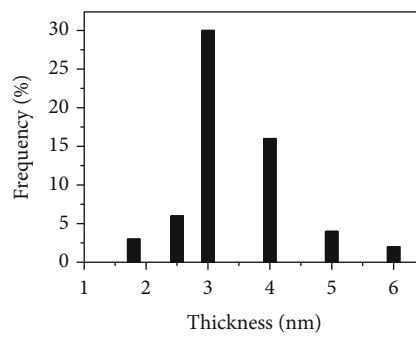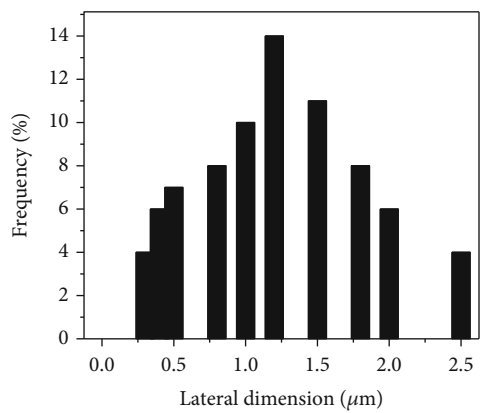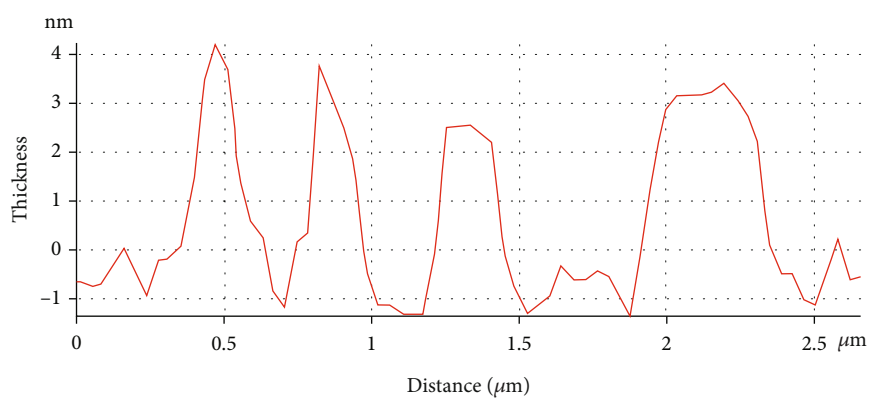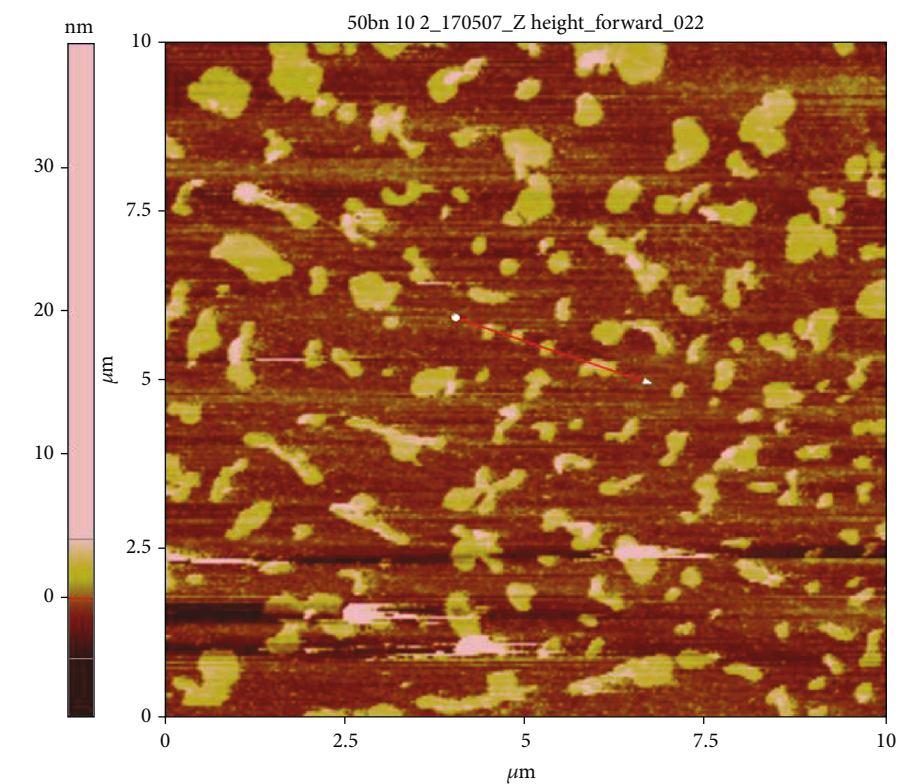
(a)

(b)

(c)

(d)

FIGURE 4: AFM image for a representative BN/APPG (a). (b) The corresponding height profile for the BN/APPG shown in (a). (c) The lateral size distribution of the BN/APPG. (d) The average results of the BN/APPG thickness.

The peak at 1375 cm^{-1} was the B–N stretching vibration, whereas the peak at 800 cm^{-1} was contributed to the B–N bending vibration.

These peaks also present at the same position in the spectra of BN/APPG composites, and intensity of the peak [33] increases with BN mass fraction loading. These results demonstrated that the APP-G polymers have been assembled on h-BN nanosheets after exfoliation, which can be explained by the formation of hydrogen bonds and π-π stacking between APPG and BN [34, 35]. UV-vis spectrometer was further applied in order to confirm the binding of the new supramolecular polymer to BN nanosheet. As shown in Figure 2(b), the UV absorption bands were positioned at 262 nm for BN/APPG/Ag with various concentrations, originating from the $\pi \rightarrow \pi *$ transitions of double bond within the adenine moieties of APPG [36]. The strength of bands becomes intensified, as the concentration of BN/APPG/Ag dispersion scales up, indicating that there is a possible functionalization of sheets with high-density supramolecular polymer. However, the absorption peak did not appear for h-BN composite. The multifunctional groups of the polymer coated the surface suitable to conjugate the Ag nanoparticles [37].

We moreover applied Raman spectroscopy in order to know the microstructure lattice vibration change of BN before and after functionalization of boron nitride. As shown Figure 3(a), the intensity of the Raman peak reduced for BN/APPG composite as result of morphological change because of functionalization and lattice disorder of boron nitride nanosheet [38].

In addition, the decrease of Raman spectrum of BN/APPG indicates the losing of Vander Waals force in the boron nitride layers and increases the interlayer spacing of the BN. In Figure 3(b), Raman spectrum of new synthesized APPG displays peaks at different wave numbers ranging from 500 to 1800 cm^{-1} which indicate that the polymer is semicrystalline gel-like carbon nanomaterials. Raman peaks with strong intensity were appeared at 70 and 130 cm^{-1} and many weak peaks were also observed. Furthermore, we used microscopy techniques to characterize morphology and microstructure of the synthesized catalyst. Field emission scanning electron microscope (FE-SEM) was applied to illustrate the difference of h-BN and BN/APPG/Ag nanomaterials in terms of morphology, size, and chemical compositions (Figure 1). The pristine BN before exfoliation shows smooth highly stacked or aggregated layers with around 1 μm thickness and large lateral dimension (Figure 1(a)). Figure 1(b) shows the BN/APPG/Ag nanomaterial that have rough surface due to modification by polymer of an Ag NPs [39]. Moreover, the nanosheets showed an average thickness of ~3.5 nm (consistent with AFM result) and average lateral dimension of ~0.1-1 μm. The EDx presented in Figure 1(d) more approves that the polymer and Ag NPs are observed over the BN nanosheet surface as compared to pristine BN (Figure 1(c)) because the N, C, O, and Ag appeared on the BN surface. The coordination of the Ag nanoparticles with polymer chain increases sustainable dispersion stability of modified BN/APPG sheet
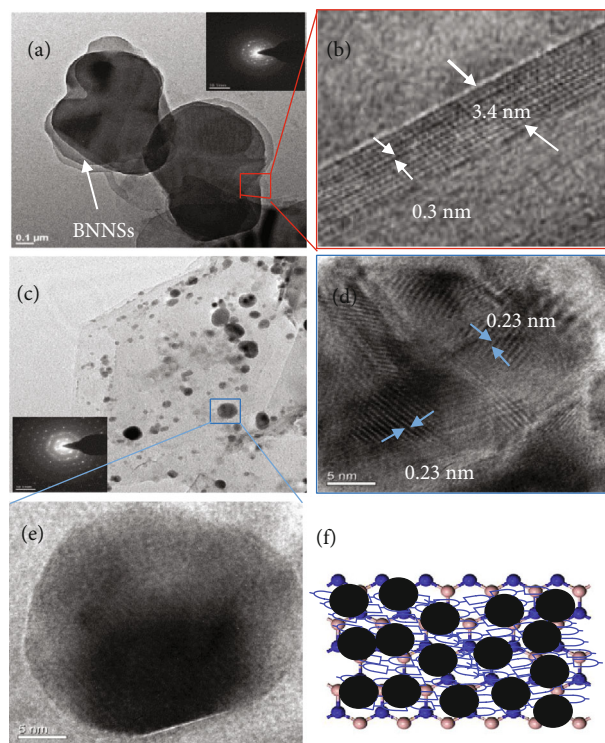

FIGURE 5: HR-TEM image of h-BN/APPG (a). Inset in (a) shows the selected area electron diffraction. (b) Sheet thickness enlarged from panel (a). (c) h-BN/APPG/Ag after deposition of Ag NPs. Inset in (c) shows the selected area electron diffraction. (d) Microstructure lattice spacing of Ag nanoparticles. (e) Enlarged view of Ag NPs from (c). (f) Schematic illustration of the new framework for hybrid catalyst of BN nanosheet-APPG-Ag nanoparticles.

for wide application in catalysis, medicine, energy, and chemical science [40].

Furthermore, we used atomic force microscopy (AFM) to measure the thickness and lateral dimension of BN/APPG nanosheet. Figure 4(a) shows the AFM image of the exfoliated BN nanosheets.

It can be observed that the functionalized BNNSs have a two-dimensional shape of nanomaterial. The lateral size of average BNNSs was in the range of 0.1–0.5 μm (Figure 4(c)). We further measured the height profile of three sheets (Figure 4(b)); the thickness ranges from 2.0 to 3.5 nm. Furthermore, the average thickness of 126 BN sheets was measured by AFM and their thickness distribution is revealed in Figure 4(d). It is found that the resultant BNNSs have a thickness predominately in the range of 3.00 nm, which includes the thickness layers of polymer layer with 80.5% of the flakes. The thickness was slightly amplified compared with the previous reports as a result of successful deposition of APPG onto the surface of BN and formed ultrathin heterogeneous multilayered surface of nanocomposites [41, 42]. BN/APPG/Ag nanocomposites were considered as a promising wastewater treatment material. Bulk boron nitrides are directly exfoliated by liquid phase sonication method in aqueous solution and as the same time noncovalently functionalized with the assistance
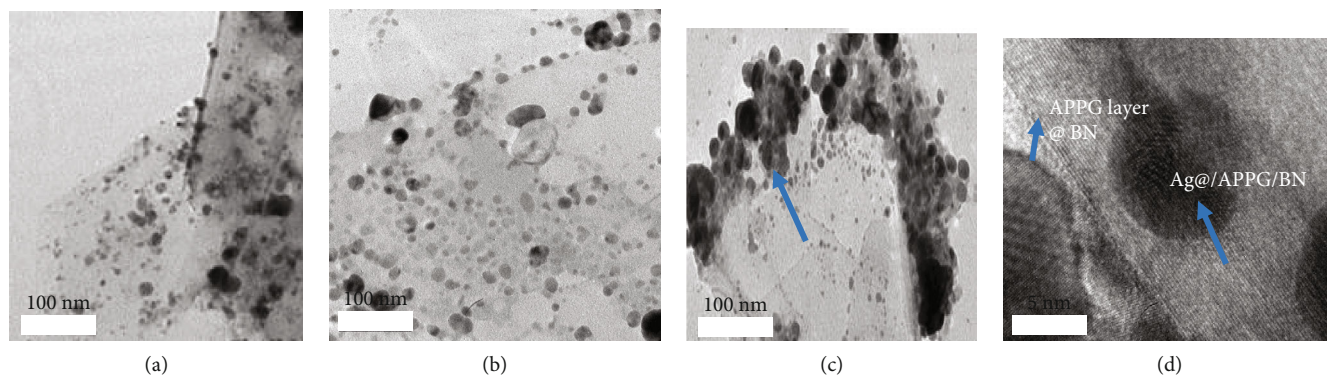
FIGURE 6: The HR-TEM image of Ag NPs on bare BN (a), BN/APPG (1 : 1) (b), and BN/APPG (1 : 2.5) (c). The enlarged view showing the Ag NPs on APPG/BN sheet (d).

of APPG [43]; then, Ag NPs were deposited on APPG/BN via conjugation polymer chains. Higher-resolution TEM was used to analyze the BN nanosheets before and after the deposition of Ag NPs and examine the role of polymer for the precipitation density of NPs (Figure 5). The observable few layer in BNNSs could be briefly revealed, in which the top layers are transparent to see the bottom layers (Figure 5(a)), and the thickness of layer could be analyzed by measuring the folded edged. The measured thickness is from 2.5 to 3.5 nm, which corresponds to few layer within sheet shown in Figure 5(b). This is further confirmed by the selected area electron diffraction (SAED) pattern shown in the inset of Figure 5(a) for the BNNSs, which exhibits a highly symmetrical ordered hexagonal structure with a 0.32 nm lattice (Figure 5(b)) distance indicating that the resultant BNNSs have thickness of 3.4 nm and are free of structural defects. TEM image in Figure 5(c) shows that the spherical Ag NPs are largely and uniformly deposited over the surface of BN. The supramolecular polymer is applied to conjugate BN nanosheet and Ag nanoparticle. Nitrogen containing groups in adenine from N-Ag bonds [26, 44]. Inset in Figure 5(c) demonstrates that the selected area electron diffraction (SAED) revealed the typical sixfold symmetry of h-BN, which demonstrates that the nanosheets are well-crystallized and not damaged during the synthesis process of BN/APPG/Ag hybrid nanomaterial. Ag NPs may not affect the microstructure of BN nanosheet supporting materials. The lattice spacing of for Ag NPs in the hybrid image is around 0.23 nm (Figure 5(d)).

Figure 5(e) shows the spherical shape of single Ag NPs deposited over BN/APPG nanosheet. Figure 5(f) shows schematic illustration of the new framework for hybrid catalyst of BNNS-APPG-Ag nanomaterial. BN/APPG/Ag complex was an effective and reusable catalyst for the degradation of RB 221 via reduction reaction. As 2D nanomaterial design system, we developed nanomaterial-like nanosheet-polymer-nanoparticle layer by layer, and the APPG polymer chain found at the middle is assumed to connect the BN sheet and Ag nanoparticle. The HR-TEM is also used to analyze Ag NP deposition over the BN surface that is functionalized and modified with different amounts of APPG polymer (Figure 6) used for the preparation of composites (bare BN and BN/APPG at different amounts of APPG),

investigating the Ag NP binding capability of the APPG polymer to grow it on BN surface. Figure 6(a) presents that the coverage spacing of the Ag NPs on bar BN is much scattered without the use of APPG polymer. When the ratio is 1 : 1, only numerous Ag NPs can be produced on the BN/APPG surface (Figure 6(b)), whereas the BN/APPG surface is almost totally covered by the Ag NPs when the ratio is grown up to 1 : 2.5 (Figure 6(c)).

The Ag NP can clearly be distinguished from the h-BN nanosheets by shape and contrast. It also should be noted that the size of the formed Ag NPs does not significantly change after being deposited onto the BN/APPG (Figure S1). In Figure 6(d), the HR-TEM image shows the Ag NPs deposited over the lamellar microstructure of APPG polymer placed functionalized on BN nanosheet. The polymeric chain, pendant group of the adenine ring system, amine, imine, and carbonyl reaction responsible groups, has the tendency to conjugate NPs due to the electrostatic interaction, oxidation/reduction, or electron transfer [24]. It is seen that the aggregation and coverage of the Ag nanoparticles can be controlled by the concentration of APPG. Our synthetic method of the newly developed BN/APPG/Ag nanocomposite will be widely studied and increase the prospective catalyst on the way to the removal of dye by tuning polymer functionalization.

3.1. Catalytic Activity. The catalytic performance of BN/Ag, APPG/Ag, BN/APPG-Ag (1 : 1), and BN/APPG-Ag (1 : 2.5) composite catalysts were investigated in terms of decolorization/reduction reaction of RB 221 (Figure 7). Figures 7(a)–7(c) and figure (S3) show the absorption spectra of RB 221 after successive adsorption reactions of dye with different catalysts observed. After addition of the catalysts, the intensity of the absorption peak positioned at 600 nm gradually became small with the reduction of dye concentration in solution proceeded. For catalysts, APPG (figure S3), BN/Ag, APPG/Ag, BNAPPG/Ag (1 : 1), and BN/APPG/Ag (1 : 2.5), adsorption of RB 221 by reduction reaction took a time of 90, 80, 60, 50, and 30 min, respectively. BN/APPG/Ag with high concentration of APPG polymer shows the highest dye removal performance compared to others [45]. In addition, the absorption peak of the RB 221 in solution
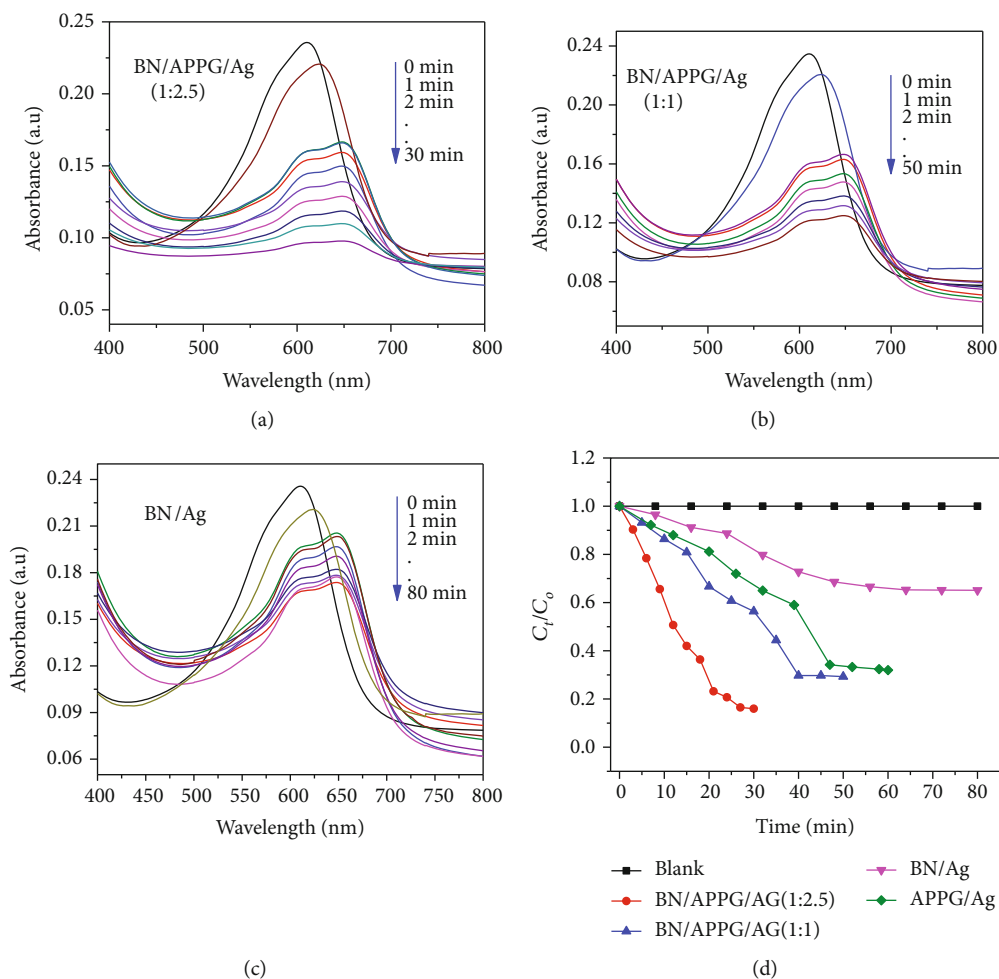
(a)

(b)

(c)

(d)

Figure 7: The time-dependent successive reduction of RB 221 over (a) BN/APPG/Ag (1 : 2.5), (b) BN/APPG/Ag (1 : 1), and (c) BN/Ag composite catalysts. (d) Plots of C_t/C_0 versus reaction time (min) for reduction of RB 221 with (a) BN/APPG/Ag (1 : 2.5), (b) BN/APPG/Ag (1 : 1), and (c) BN/Ag. (c) APPG/Ag (Fig.S2) composite catalysts.

undergo upshifts (~40 nm difference) relative to the free dye indicating the reduction of RB 221 dye with BN/AG and BN/APPG/Ag catalysts by disruption of electronic structure. The shifting of peaks to the right is insignificant as increasing UV irradiation time. Unfortunately, the upshift did not appear for APPG and APPG/Ag catalyst (figure S2); it could be concluded that the upshift corresponds to the degradation of dye by BN nanosheets [17, 46, 47]. During light irradiation, absorption of photons takes place and leads to the formation of charge separation due to the electron excitation from the valence band of the APPG-functionalized BN nanosheet. Due to the Fermi level equilibration, the charge recombination of pairs was reduced and used for degradation purpose. The higher photocatalytic activity for the degradation of RB 221 under the direct sunlight can also be attributed to the synergistic effect of plasmonic absorption from the surface plasma resonance of Ag NPs and the enhanced adsorption capacity for RB 221.

Figure 7(d) shows the plots of C_t/C_0 concentration ratio as a function of reaction time (t) between RB 221 dye and catalysts, where C_0 and C_t correspond to the initial concen-

tration and the concentration at time (t). The percent removal of RB 221 dye by catalyst from aqueous solution was calculated by equation (1). As it is observed in Figure 7(d), the dye removal efficiency of synthesized catalysts such as BN/APPG/Ag (1 : 2.5), BN/APPG/Ag (1.1), APPG/Ag (figure S2), and BN/Ag were 84.60 ± 1.26, 70.13 ± 0.034, 65.60 ± 0.052, and $35.0 \pm 0.045\%$, respectively [48–50] [51]. The comparison of the catalytic activity of BN/APPG/Ag composite catalyst with the related reported catalysts used for the reduction of RB 221 is shown in Table 1. BN/APPG/Ag with high amount of polymer shows highest photocatalytic dye removal efficiency because adenine-functionalized polymer was significantly higher than that of BN/Ag [52, 53]. Indeed, the presence of the adenine functional groups on h-BNNSs induces and increases the formation of Ag NPs through Ag/adenine moiety coordination; as a result, there were many ways of possible interactions between the heterogeneous catalyst, and therefore, the photocatalyst activity of BN/APPG/Ag was the highest for removal of RB 221 [15, 50, 54, 55].

The dye removal ability of the best catalyst (BN/APPG/Ag) with high amount of APPG was retested for three cycles

TABLE 1: Comparison of the degradation effect of various photocatalytic catalysts reported in literature for the removal of RB 221 from aqueous solution [51, 56–58].

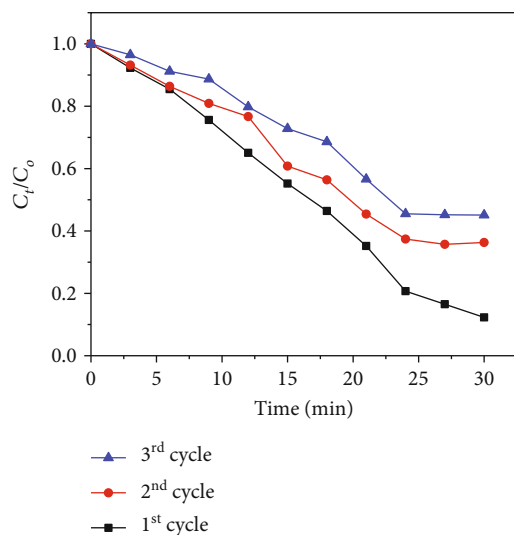| No.	Catalysts	Removal of RB 221 (%)	References
1.	ZnO_2/PEG	81.69	46
2.	HRP in Ca-alginate beads	73	45
3.	Microalgae PSU-NFW	30.20	40
4.	BN/APPG/Ag	84.6	This study

FIGURE 8: Reusability for three cycles of BN/APPG/Ag catalysts towards decolorization of RB 221.

of reusability of catalyst to remove RB 221 (Figure 8). For the first cycles of catalytic reduction of dye performed, the removal percentage of dyes was $83.7 \pm 0.8\%$. For the second cycle of regeneration, percent removal of RB 221 was $63.8 \pm 0.5\%$. For the third regeneration cycle, the removal percentage of RB 221 was $54.60 \pm 0.78\%$. It is also recognized that the performance of the catalyst gradually decreases for the increased number of cycles. [49, 56, 59] However, the overall removal percentage of RB 221 dye suggests that it can sustain its removal capability with numerous cycles of reuse and may be applied repetitively for dye removal of organic contaminate dyes from wastewater in the environment [18, 60].

4. Conclusions

In conclusion, we have established the protocol to form supramolecular BN nanosheets in order to induce catalytic silver nanoparticle deposition. Supramolecular polymer that is noncovalently bond to the BNNS surface is able to assist the creation of catalytic NPs. BNNSs can be applied an effective catalyst support because of their chemical inertness and high specific surface area. Our preparation method shows that BNNSs might develop novel nanomaterials with tuning

their functionalization to the formation of the blend of complex systems; this technique is valuable for the cost-effective and controlled design of new catalysts and for the fabrication of advanced devices by using BNNSs. Moreover, we have investigated the removal percentage of RB 221 using BN/APPG/Ag nanomaterial, which was efficient heterogeneous catalyst and the reusability of regenerated catalyst that does show significant reduction in catalytically removal of RB 221 over several recycles. The reported designed platform is a promising approach of processing for engineering this novel layered material, paving the means for a diversity of catalysis, electronics, drug delivery, and nanocomposite-related applications.

Data Availability

Almost all image and spectra data of sample data used to support the findings of this study are included within the article. The reusability dye degradation effects of APPG and APPG/Ag used to support the findings of this study are included within the supplementary information file(s). The APPG experimental data used to support the findings of this study are currently under embargo while the research findings are commercialized. Previously reported Ag and BN data used to support this study are cited at relevant places within the text as references. The data supporting this research are from previously reported studies which have been cited. The APPG data used to support the findings of this study are available from the corresponding author upon request.

Conflicts of Interest

The authors declare no conflicts of interest.

Acknowledgments

Supplementary Materials

Figure S1 shows the growth of Ag NPs over substrate without supportive materials (BNSSs) and supramolecular polymer (APPG). Very few particles deposited as compared to the particles observed over supramolecular BN nanosheets. So the density of the Ag NP increases by BN substrate and polymer absorbers. However, the size of the formed Ag NPs does not significantly change after being deposited onto the BN/APPG (Figure 6). Figures S2 and S3 show the decolorization/degradation of efficiency of APPG/Ag and APPG polymer against RB 221 at time interval. After addition of the APPG and APPG/Ag, the intensity of the absorption peak positioned at 600 nm gradually became small with the reduction of dye concentration in solution proceeded. For catalysts, APPG, and APPG/Ag, adsorption of RB 221 by

reduction reaction took a time of 90 and 60 min, respectively. APPG/Ag show high relativity to pure polymer due to Ag catalyst. Generally, APPG and APPG/Ag reveal low degradation efficiency relative to BN/APPG/Ag. Figure S1: high-resolution TEM image of pure Ag Nanoparticles. Figure S2: the time-dependent successive adsorption of RB221 over APPG-Ag catalyst. Figure S3: the time-dependent successive adsorption of RB221 over APPG catalysts. *(Supplementary Materials)*

References

[1] I. Y. Zhitnyak, I. N. Bychkov, I. V. Sukhorukova et al., "Effect of BN nanoparticles loaded with doxorubicin on tumor cells with multiple drug resistance," *ACS Applied Materials & Interfaces*, vol. 9, no. 38, pp. 32498–32508, 2017.

[2] H. Zhu, Y. Li, Z. Fang et al., "Highly thermally conductive papers with percolative layered boron nitride nanosheets," *ACS Nano*, vol. 8, no. 4, pp. 3606–3613, 2014.

[3] X. Cui, P. Ding, N. Zhuang, L. Shi, N. Song, and S. Tang, "Thermal conductive and mechanical properties of polymeric composites based on solution-exfoliated boron nitride and graphene nanosheets: a morphology-promoted synergistic effect," *ACS Applied Materials & Interfaces*, vol. 7, no. 34, pp. 19068–19075, 2015.

[4] C.-C. Cheng, A. A. Muhabie, S.-Y. Huang et al., "Dual stimuli-responsive supramolecular boron nitride with tunable physical properties for controlled drug delivery," *Nanoscale*, vol. 11, no. 21, pp. 10393–10401, 2019.

[5] G. Eda, T. Fujita, H. Yamaguchi, D. Voiry, M. Chen, and M. Chhowalla, "Coherent atomic and electronic heterostructures of single-layer MoS2," *ACS Nano*, vol. 6, no. 8, pp. 7311–7317, 2012.

[6] A. Y. S. Eng, A. Ambrosi, Z. Sofer, P. Šimek, and M. Pumera, "Electrochemistry of transition metal dichalcogenides: strong dependence on the metal-to-chalcogen composition and exfoliation method," *ACS Nano*, vol. 8, no. 12, pp. 12185–12198, 2014.

[7] S. S. Chou, N. Sai, P. Lu et al., "Understanding catalysis in a multiphasic two-dimensional transition metal dichalcogenide," *Nature Communications*, vol. 6, no. 1, p. 8311, 2015.

[8] Y. Chen, D. Ye, M. Wu et al., "Break-up of two-dimensional MnO_2 nanosheets promotes ultrasensitive pH-triggered theranostics of cancer," *Advanced Materials*, vol. 26, no. 41, pp. 7019–7026, 2014.

[9] A. A. Muhabie, C.-C. Cheng, J.-J. Huang et al., "Non-covalently functionalized boron nitride mediated by a highly self-assembled supramolecular polymer," *Chemistry of Materials*, vol. 29, no. 19, pp. 8513–8520, 2017.

[10] A. Amiri, M. Naraghi, G. Ahmadi, M. Soleymaniha, and M. Shanbedi, "A review on liquid-phase exfoliation for scalable production of pure graphene, wrinkled, crumpled and functionalized graphene and challenges," *FlatChem*, vol. 8, pp. 40–71, 2018.

[11] L. Cheng, J. Liu, X. Gu et al., "Imaging: PEGylated WS2Nanosheets as a multifunctional theranostic agent for in vivo dual-modal CT/photoacoustic imaging guided photothermal therapy (Adv. Mater. 12/2014)," *Advanced Materials*, vol. 26, no. 12, p. 26, 2014.

[12] D. Deng, K. S. Novoselov, Q. Fu, N. Zheng, Z. Tian, and X. Bao, "Catalysis with two-dimensional materials and their heterostructures," *Nature Nanotechnology*, vol. 11, no. 3, pp. 218–230, 2016.

[13] D. A. Henckel, O. Lenz, and B. M. Cossairt, "Effect of ligand coverage on hydrogen evolution catalyzed by colloidal WSe2," *ACS Catalysis*, vol. 7, no. 4, pp. 2815–2820, 2017.

[14] L. S. Zhong, J. S. Hu, H. P. Liang, A. M. Cao, W. G. Song, and L. J. Wan, "Self-assembled 3D flowerlike iron oxide nanostructures and their application in water treatment," *Advanced Materials*, vol. 18, no. 18, pp. 2426–2431, 2006.

[15] P. Singh, G. Lamanna, C. Ménard-Moyon et al., "Formation of efficient catalytic silver nanoparticles on carbon nanotubes by adenine functionalization," *Angewandte Chemie International Edition*, vol. 50, no. 42, pp. 9893–9897, 2011.

[16] S. Singh, P. K. Singh, and H. Mahalingam, "Novel floating Ag+-doped TiO2/polystyrene photocatalysts for the treatment of dye wastewater," *Industrial & Engineering Chemistry Research*, vol. 53, no. 42, pp. 16332–16340, 2014.

[17] J. Zhang, G. Chen, M. Chaker, F. Rosei, and D. Ma, "Gold nanoparticle decorated ceria nanotubes with significantly high catalytic activity for the reduction of nitrophenol and mechanism study," *Applied Catalysis B: Environmental*, vol. 132, pp. 107–115, 2013.

[18] M. T. Yagub, T. K. Sen, S. Afroze, and H. M. Ang, "Dye and its removal from aqueous solution by adsorption: a review," *Advances in Colloid and Interface Science*, vol. 209, pp. 172–184, 2014.

[19] C. Y. Teh, P. M. Budiman, K. P. Y. Shak, and T. Y. Wu, "Recent advancement of coagulation–flocculation and its application in wastewater treatment," *Industrial & Engineering Chemistry Research*, vol. 55, no. 16, pp. 4363–4389, 2016.

[20] J. Liu, L. Han, H. Ma et al., "Template-free synthesis of carbon doped TiO_2 mesoporous microplates for enhanced visible light photodegradation," *Science Bulletin*, vol. 61, no. 19, pp. 1543–1550, 2016.

[21] Y. Xie, B. Yan, H. Xu et al., "Highly regenerable mussel-inspired Fe3O4@ polydopamine-Ag core–shell microspheres as catalyst and adsorbent for methylene blue removal," *ACS Applied Materials & Interfaces*, vol. 6, no. 11, pp. 8845–8852, 2014.

[22] B. R. Ganapuram, M. Alle, R. Dadigala, A. Dasari, V. Maragoni, and V. Guttena, "Catalytic reduction of methylene blue and Congo red dyes using green synthesized gold nanoparticles capped by salmalia malabarica gum," *International Nano Letters*, vol. 5, no. 4, pp. 215–222, 2015.

[23] Z. Gan, A. Zhao, M. Zhang et al., "Controlled synthesis of Au-loaded Fe 3 O 4@ C composite microspheres with superior SERS detection and catalytic degradation abilities for organic dyes," *Dalton Transactions*, vol. 42, no. 24, pp. 8597–8605, 2013.

[24] A. A. Muhabie, C.-H. Ho, B. T. Gebeyehu et al., "Dynamic tungsten diselenide nanomaterials: supramolecular assembly-induced structural transition over exfoliated two-dimensional nanosheets," *Chemical Science*, vol. 9, no. 24, pp. 5452–5460, 2018.

[25] W. Baran, A. Makowski, and W. Wardas, "The separation of catalyst after photocatalytic reactions conducted in the presence of $TiO_2/FeCl_3/UV$," *Chemosphere*, vol. 59, no. 6, pp. 853–859, 2005.

[26] S. R. Sushrutha, R. Hota, and S. Natarajan, "Adenine-based coordination polymers: synthesis, structure, and properties," *European Journal of Inorganic Chemistry*, vol. 2016, no. 18, pp. 2962–2974, 2016.

[27] C.-C. Cheng, J.-J. Huang, A. A. Muhable et al., "Supramolecular fluorescent nanoparticles functionalized with controllable physical properties and temperature-responsive release behavior," *Polymer Chemistry*, vol. 8, no. 15, pp. 2292–2298, 2017.

[28] C.-C. Cheng, F.-C. Chang, H.-C. Yen, D.-J. Lee, C.-W. Chiu, and Z. Xin, "Supramolecular assembly mediates the formation of single-chain polymeric nanoparticles," *ACS Macro Letters*, vol. 4, no. 10, pp. 1184–1188, 2015.

[29] W. Mamdouh, M. Dong, S. Xu, E. Rauls, and F. Besenbacher, "Supramolecular nanopatterns self-assembled by adenine−thymine quartets at the liquid/solid interface," *Journal of the American Chemical Society*, vol. 128, no. 40, pp. 13305–13311, 2006.

[30] Y. Wu, Y. Xue, S. Qin et al., "BN nanosheet/polymer films with highly anisotropic thermal conductivity for thermal management applications," *ACS Applied Materials & Interfaces*, vol. 9, no. 49, pp. 43163–43170, 2017.

[31] C.-C. Cheng, F.-C. Chang, J.-H. Wang et al., "Large-scale production of ureido-cytosine based supramolecular polymers with well-controlled hierarchical nanostructures," *RSC Advances*, vol. 5, no. 93, pp. 76451–76457, 2015.

[32] M. Hayashi and F. Tournilhac, "Thermal stability enhancement of hydrogen bonded semicrystalline thermoplastics achieved by combination of aramide chemistry and supramolecular chemistry," *Polymer Chemistry*, vol. 8, no. 2, pp. 461–471, 2017.

[33] D. Golberg, Y. Bando, Y. Huang et al., "Boron nitride nanotubes and nanosheets," *ACS Nano*, vol. 4, no. 6, pp. 2979–2993, 2010.

[34] J. Gu, X. Yang, Z. Lv, N. Li, C. Liang, and Q. Zhang, "Functionalized graphite nanoplatelets/epoxy resin nanocomposites with high thermal conductivity," *International Journal of Heat and Mass Transfer*, vol. 92, pp. 15–22, 2016.

[35] P. Thangasamy, M. Santhanam, and M. Sathish, "Supercritical fluid facilitated disintegration of hexagonal boron nitride nanosheets to quantum dots and its application in cells imaging," *ACS Applied Materials & Interfaces*, vol. 8, no. 29, pp. 18647–18651, 2016.

[36] T. Feng, X. Ai, H. Ong, and Y. Zhao, "Dual-responsive carbon dots for tumor extracellular microenvironment triggered targeting and enhanced anticancer drug delivery," *ACS Applied Materials & Interfaces*, vol. 8, no. 29, pp. 18732–18740, 2016.

[37] M. S. Strozyk, M. Chanana, I. Pastoriza-Santos, J. Pérez-Juste, and L. M. Liz-Marzán, "Protein/polymer-based dual-responsive gold nanoparticles with pH-dependent thermal sensitivity," *Advanced Functional Materials*, vol. 22, no. 7, pp. 1436–1444, 2012.

[38] K. N. Kudin, B. Ozbas, H. C. Schniepp, R. K. Prud'Homme, I. A. Aksay, and R. Car, "Raman spectra of graphite oxide and functionalized graphene sheets," *Nano Letters*, vol. 8, no. 1, pp. 36–41, 2008.

[39] S. Velayudham, C. H. Lee, M. Xie et al., "Noncovalent functionalization of boron nitride nanotubes with poly(p-phenylene-ethynylene)s and polythiophene," *ACS Applied Materials & Interfaces*, vol. 2, no. 1, pp. 104–110, 2010.

[40] W. Lei, D. Liu, and Y. Chen, "Highly crumpled boron nitride nanosheets as adsorbents: scalable solvent-less production," *Advanced Materials Interfaces*, vol. 2, no. 3, p. 1400529, 2015.

[41] A. Lyalin, A. Nakayama, K. Uosaki, and T. Taketsugu, "Functionalization of monolayer h-BN by a metal support for the oxygen reduction reaction," *The Journal of Physical Chemistry C*, vol. 117, no. 41, pp. 21359–21370, 2013.

[42] C. Huang, C. Chen, X. Ye et al., "Stable colloidal boron nitride nanosheet dispersion and its potential application in catalysis," *Journal of Materials Chemistry A*, vol. 1, no. 39, pp. 12192–12197, 2013.

[43] Z. Gao, C. Zhi, Y. Bando, D. Golberg, and T. Serizawa, "Noncovalent functionalization of boron nitride nanotubes in aqueous media opens application roads in nanobiomedicine," *Nano*, vol. 1, p. 7, 2014.

[44] A. R. Deshmukh, H. Aloui, and B. S. Kim, "In situ growth of gold and silver nanoparticles onto phyto-functionalized boron nitride nanosheets: catalytic, peroxidase mimicking, and antimicrobial activity," *Journal of Cleaner Production*, vol. 270, article 122339, 2020.

[45] J. Pang, Y. Chao, H. Chang et al., "Silver nanoparticle-decorated boron nitride with tunable electronic properties for enhancement of adsorption performance," *ACS Sustainable Chemistry & Engineering*, vol. 6, no. 4, pp. 4948–4957, 2018.

[46] A. R. Deshmukh and B. S. Kim, "Bio-functionalized few-layer graphene for in situ growth of gold nanoparticles, improvement of polymer properties, and dye removal," *Journal of Cleaner Production*, vol. 310, p. 127515, 2021.

[47] H. Li, D. Jiang, Z. Huang et al., "Preparation of silver-nanoparticle-loaded magnetic biochar/poly (dopamine) composite as catalyst for reduction of organic dyes," *Journal of Colloid and Interface Science*, vol. 555, pp. 460–469, 2019.

[48] F. Ali, S. B. Khan, T. Kamal, K. A. Alamry, and A. M. Asiri, "Chitosan-titanium oxide fibers supported zero-valent nanoparticles: highly efficient and easily retrievable catalyst for the removal of organic pollutants," *Scientific Reports*, vol. 8, no. 1, pp. 1–18, 2018.

[49] M. H. Karaoglu, M. Dogan, and M. Alkan, "Removal of reactive blue 221 by kaolinite from aqueous solutions," *Industrial & Engineering Chemistry Research*, vol. 49, no. 4, pp. 1534–1540, 2010.

[50] C.-W. Chiu, M.-T. Wu, C.-L. Lin et al., "Adsorption performance for reactive blue 221 dye of β-chitosan/polyamine functionalized graphene oxide hybrid adsorbent with high acid–alkali resistance stability in different acid–alkaline environments," *Nanomaterials*, vol. 10, no. 4, p. 748, 2020.

[51] N. O. San Keskin, A. Celebioglu, T. Uyar, and T. Tekinay, "Microalgae immobilized by nanofibrous web for removal of reactive dyes from wastewater," *Industrial & Engineering Chemistry Research*, vol. 54, no. 21, pp. 5802–5809, 2015.

[52] T. Bhowmik, M. K. Kundu, and S. Barman, "Ultra small gold nanoparticles–graphitic carbon nitride composite: an efficient catalyst for ultrafast reduction of 4-nitrophenol and removal of organic dyes from water," *RSC Advances*, vol. 5, no. 48, pp. 38760–38773, 2015.

[53] B. Guo, Q. Li, J. Lin et al., "Bimetallic AuPd nanoparticles loaded on amine-functionalized porous boron nitride nanofibers for catalytic dehydrogenation of formic acid," *ACS Applied Nano Materials*, vol. 4, no. 2, pp. 1849–1857, 2021.

[54] T. K. Das, S. Ganguly, P. Bhawal, S. Remanan, S. Mondal, and N. Das, "Mussel inspired green synthesis of silver nanoparticles-decorated halloysite nanotube using dopamine: characterization and evaluation of its catalytic activity," *Applied Nanoscience*, vol. 8, no. 1-2, pp. 173–186, 2018.

[55] H. Gholami Derami, P. Gupta, R. Gupta, P. Rathi, J. J. Morrissey, and S. Singamaneni, "Palladium nanoparticle-decorated mesoporous polydopamine/bacterial nanocellulose as a catalytically active universal dye removal ultrafiltration membrane," *ACS Applied Nano Materials*, vol. 3, no. 6, pp. 5437–5448, 2020.

[56] M. Alkan, S. Çelikçapa, Ö. Demirbaş, and M. Doğan, "Removal of reactive blue 221 and acid blue 62 anionic dyes from aqueous solutions by sepiolite," *Dyes and Pigments*, vol. 65, no. 3, pp. 251–259, 2005.

[57] S. Farias, D. A. Mayer, D. de Oliveira, S. de Souza, and A. A. U. de Souza, "Free and Ca-alginate beads immobilized horseradish peroxidase for the removal of reactive dyes: an experimental and modeling study," *Applied Biochemistry and Biotechnology*, vol. 182, no. 4, pp. 1290–1306, 2017.

[58] P. C. Kale and P. L. Chaudhari, "Removal of reactive blue 221 dye from textile waste water by using zinc peroxide nanoparticles," *International Journal of Scientific Research and Management*, vol. 5, pp. 5700–5709, 2017.

[59] Y. Wang, X. Wang, and M. Antonietti, "Polymeric graphitic carbon nitride as a heterogeneous organocatalyst: from photochemistry to multipurpose catalysis to sustainable chemistry," *Angewandte Chemie International Edition*, vol. 51, no. 1, pp. 68–89, 2012.

[60] X. Wang, S. Blechert, and M. Antonietti, "Polymeric graphitic carbon nitride for heterogeneous photocatalysis," *ACS Catalysis*, vol. 2, no. 8, pp. 1596–1606, 2012.